Effect of Impurity Ions on Ion Current Flowing into an Ion Sensitive Probe during N_2 and H_2 Seeding in Hydrogen Plasma

Takuma OKAMOTO, Naomichi EZUMI, Satoshi TOGO, Renato PERILLO[1)], Naoki SHIGEMATSU, Takumi SETO, Kosuke TAKANASHI, Satoshi TAKAHASHI, Reina MIYAUCHI and Mizuki SAKAMOTO

Plasma Research Center, University of Tsukuba, Tsukuba, Ibaraki 305-8577, Japan
[1)] *University of California San Diego, San Diego, CA, USA*

(Received 24 February 2023 / Accepted 13 April 2023)

We attempt to interpret the different trends of collected ion currents of the Langmuir probe and the ion sensitive probe (ISP) observed during N_2 and H_2 seeding in hydrogen plasmas in the divertor simulation experimental module (D-module) in GAMMA10/PDX. The current measured at the ion collector electrode of the ISP shows two distinct bumps. Results can be interpreted with the aid of spectroscopic measurements related to the dominant reaction processes, where nitrogen-induced molecule-activated-recombination (N-MAR) mechanisms produce various ion species, resulting in different measured currents. These experimental findings provide a further understanding of the most relevant plasma-neutral processes occurring in a detached-like plasma scenario in the presence of nitrogen, a candidate for impurity seeding in ITER.

Keywords: divertor, ion species, Larmor radii, ion sensitive probe, MAR, atomic and molecular processes

DOI: 10.1585/pfr.18.1402047

1. Introduction

One of the challenges in building a fusion reactor is protecting divertor plates from enormous heat loads. The particle flux to the divertor must be reduced to reduce the heat load. For this purpose, forming a detached plasma through plasma-gas interaction is being considered [1, 2]. In a detached plasma, a decrease in electron temperature reduces the particle flux by volumetric recombination. Volumetric recombination is an important reaction for reducing particle flux. In particular, at relatively high electron temperatures (between ∼1 and ∼5 eV), molecular-activated recombination (MAR) dominates the radiative and three-body electron-ion recombination (EIR) [3].

Reference [4] shows that a reaction process called "nitrogen-induced MAR (N-MAR)," associated with nitrogen seeding, enhances the conversion of ions to neutral particles and makes the heat load on divertor plates more tolerable. N-MAR has higher rate coefficients over a wider electron temperature range than hydrogen-induced MAR (H-MAR), which has been experimentally demonstrated in Magnum-PSI [5, 6]. In GAMMA 10/PDX, obvious particle flux reduction is observed by the combined seeding of hydrogen and nitrogen gases [7, 8]. The beneficial role of nitrogen in plasma detachment is related to its radiative properties [9]. Nitrogen is an effective gas for reducing the heat load in the divertor section.

In Ref. [8], an experiment is conducted to investigate the effects of changing the ratio of nitrogen to hydrogen on the formation of detached plasmas during the combined seeding of hydrogen and nitrogen. The electron density and ion fluxes decrease as the ratio of nitrogen gas increases. However, the decrease in electron density is smaller than the decrease in ion flux. Reference [8] suggests that impurity ions can affect the ion flux because of their mass effect. The N-MAR reaction process produces multiple ion species. N-MAR is a chain reaction mediated by the molecular ions NH_x^+ and involves several ion species. In this study, we especially focus on an Ion Sensitive Probe (ISP) installed in a divertor simulation experimental module (D-module) [10] to focus on impurity ions produced by the N-MAR reaction. We investigate the effect of impurity ions on the ion current flowing into the ISP and compare it with spectroscopic results to estimate the impurity ions produced. Ultimately, we estimate the influence of such impurity ions on the particle flux reduction.

2. Experimental Setup

2.1 GAMMA 10/PDX

Figure 1 (a) shows a schematic view of GAMMA 10/PDX which is a large tandem mirror device. To simulate a divertor, the D-module is installed in the west end region of the device [11–14]. The plasma in the mirror confinement regions flows into the west end region along the open magnetic field lines.

Figure 1 (b) shows a schematic view of the D-module. In this module, a tungsten V-shaped target plate is installed

author's e-mail: okamoto_takuma@prc.tsukuba.ac.jp

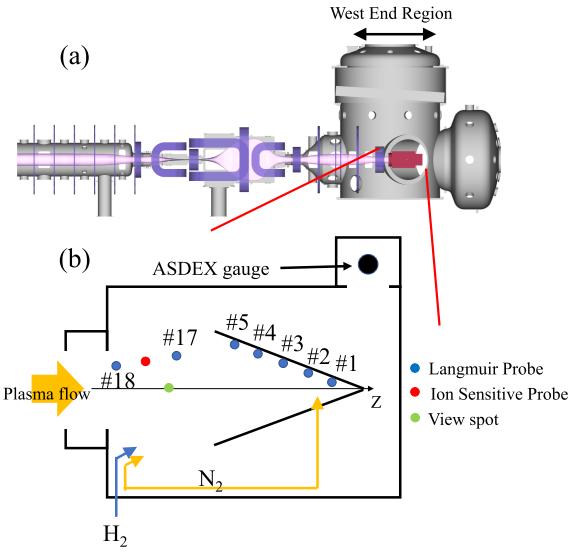

Fig. 1 Schematic views of (a) GAMMA 10/PDX and (b) the divertor simulation experimental module (D-module).

to simulate a divertor plate. Additional hydrogen gas is supplied from the inlet of the D-module and nitrogen gas is supplied from the inlet and corner of the target plate. Langmuir probes and an ISP are installed in the D-module, and spectroscopic measurements can be performed with a visible light spectrometer. An ASDEX ion gauge is installed on the top of the D-module to measure the neutral pressure in the D-module.

2.2 Influence of impurity ions on Ion Sensitive Probe

ISPs are normally used to measure the ion temperature perpendicular to the magnetic field line [15]. An ISP consists of two electrodes, a guard electrode, and an ion collector. The ion collector is deeper than the guard electrode to prevent electrons from flowing into the ion collector. ISPs are probes that collect only ions with an ion collector due to the difference in Larmor radii between electrons and ions. Here, we focus on the ion Larmor radii ρ, expressed by the following relation, where the velocity distribution of ions is assumed to be the Maxwellian distribution and the average ion thermal velocity is used;

$$\rho_s = \frac{1}{qB}\sqrt{\frac{8m_s k T_{i\perp}}{\pi}}, \tag{1}$$

where m represents the ion mass, $T_{i\perp}$ denotes the ion temperature perpendicular to the magnetic field line, q represents an elementary charge, k represents a Boltzmann constant, and B represents the magnetic field. Subscript "s" represents ion species.

The depth of the ion collector of the ISP installed in the D-module is 0.5 mm (Fig. 2 (a)). With the magnetic field $B = 0.68$ T at the ISP location and the collector electrode depth, the lower energy limit for impurity ions assumed in this experiment (N^+, $N_2{}^+$, N_2H^+, NH^+) is calculated to be less than 1 eV for all ions, as depicted in Fig. 2 (b). For hydrogen ions, the limit is 4.4 eV. This suggests that impurity ions are heavy and can reach the ion collector electrode even at low energies. Therefore, although the ion collector current depends on the total number of ions and temperature, the current is expected to increase because of impurity ions rather than hydrogen ions.

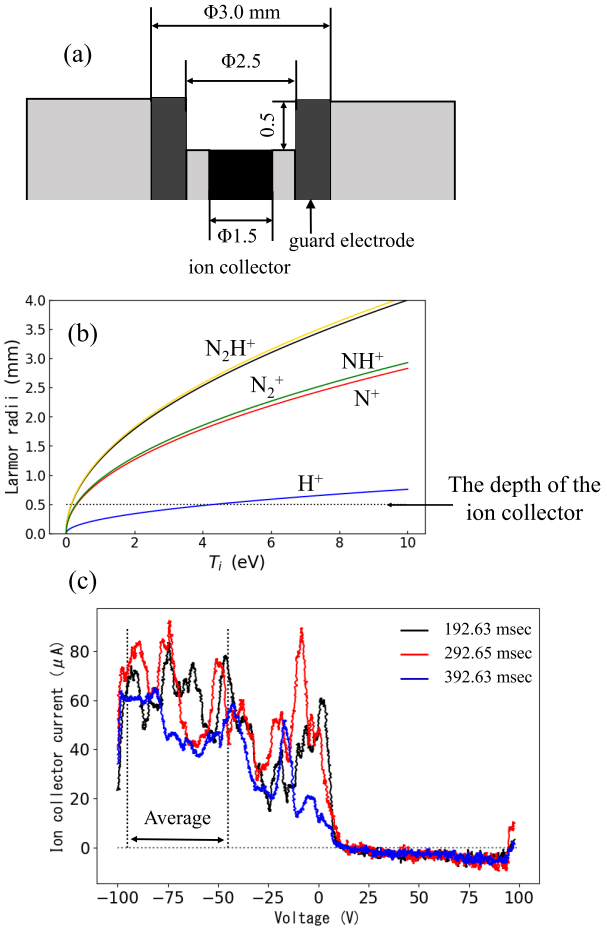

Fig. 2 (a) The structure of the ISP in the D-module, (b) comparison of Larmor radii ρ as functions of the ion temperature $T_{i\perp}$ at $B = 0.68$ T, and (c) I-V characteristics of the ISP ion collector of #252269.

A voltage ranging from −100 V to 100 V is applied to the ISP installed in the D-module. The sweep frequency is 100 Hz. A shunt resistor of 1 Ω is used for the guard electrode and 100 Ω for the ion collector electrode. The ion collector electrode is always 6.24 V lower than the guard electrode using a battery to prevent electrons from flowing into the ion collector [16]. Because the current is unstable as depicted in Fig. 2 (c), the ion collector current adopts the average when −95 to −45 V is applied, which is the ion saturation region.

3. Experimental Results and Discussion

Hydrogen plasma is generated at t = 50 ms and sustained for 400 ms. Nitrogen gas is seeded after $t \sim$ 100 ms, and additional hydrogen gas is seeded after $t \sim$ 150 ms into the D-module. The nitrogen gas pressure is adjusted to approximately 10% of the hydrogen gas pressure at the end of the discharge (Fig. 3 (a)).

Figure 3 (b) shows the time evolutions of the diamagnetism in the mirror field confinement region. The time evolutions of the diamagnetism for the three shots used in this study indicate that the plasmas are very reproducible. All Langmuir probe and ISP measurements discussed below are the averages of these three shots.

Figure 4 shows the time evolutions of (a) the ion collector current measured by the ISP, (b) the emission intensities of N^+ ($I_{N}{}^+$), $N_2{}^+$ ($I_{N2}{}^+$), and NH (I_{NH}) measured by the spectrometer, (c) the ion temperature ($T_{i\perp}$) measured by the ISP, (d) the electron temperature (T_e) measured by the Langmuir probes #3 and #17 (Fig. 1 (b)), (e) the electron density (n_e) and the ion flux (Γ_i) measured by #3, and (f) n_e and Γ_i measured by #17. Two bumps are observed in the ISP ion collector current as depicted in Fig. 4 (a). The error bars in Fig. 4 (a) are obtained from the standard error calculated from the deviation between the ion saturation current averaged over the three shots and that one for each shot. The first bump is at t = 90 - 220 ms and the second one is at t = 220 - 370 ms. To discuss the current behavior, we use time zones I ~ IV as shown in Fig. 4 (a). Zone I is defined as t = 90 - 150 ms, II as t = 150 - 220 ms, III as t = 220 - 310 ms, and IV as t = 310 - 370 ms. The trend of the result is independent of the range to take an average for the ion current in the I-V curve.

The effects of impurity ions on the ion collector cur-

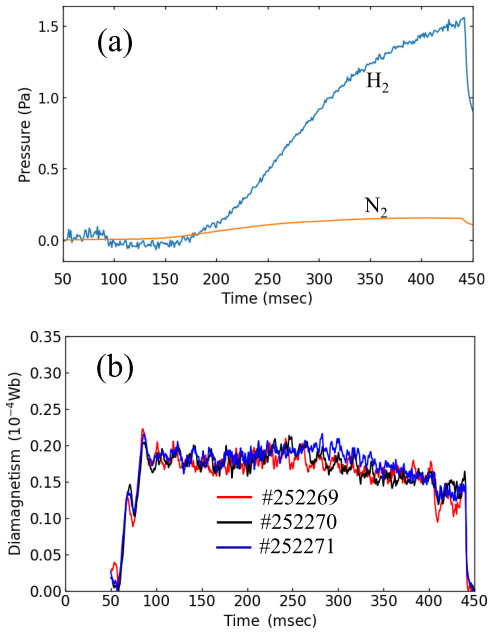

Fig. 3 Time evolutions of (a) the neutral gas pressure and (b) the diamagnetism in the magnetic confinement region.

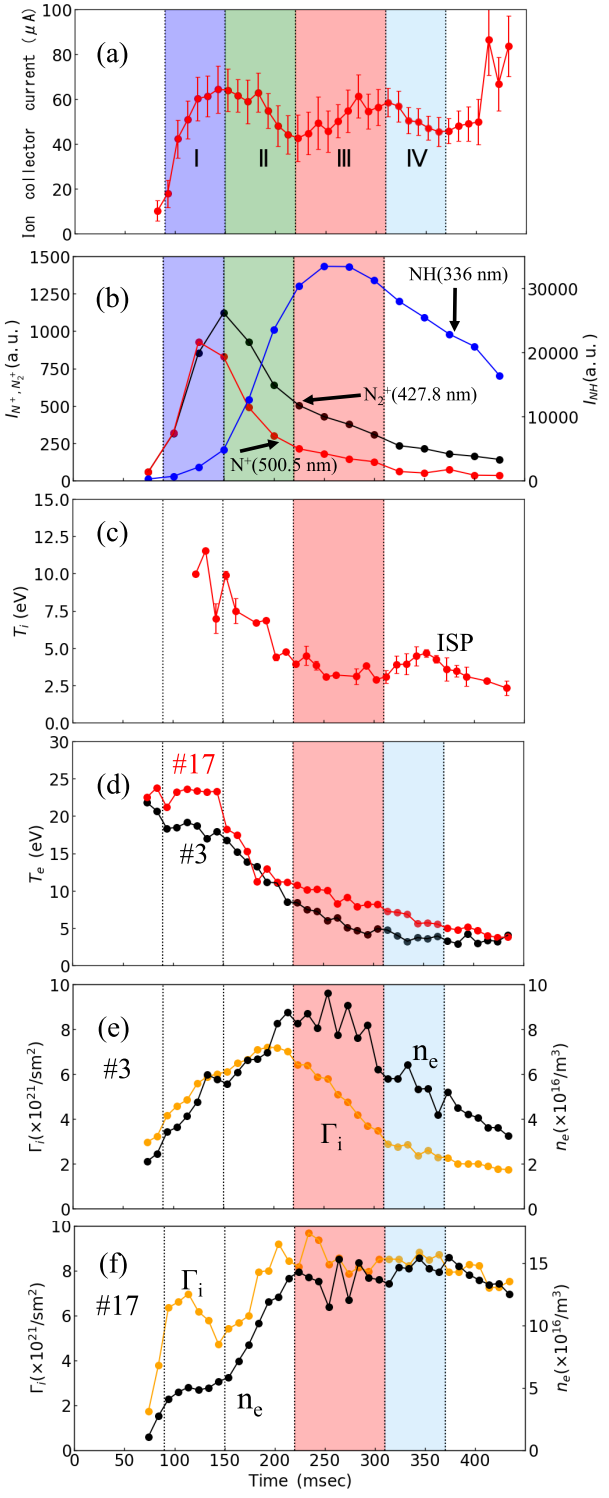

Fig. 4 Time evolutions of (a) the ion collector current (ISP), (b) the emission intensities (N^+, $N_2{}^+$, NH), (c) the ion temperature $T_{i\perp}$, (d) the electron temperature T_e (#3, #17), (e), (f) the electron density n_e and the ion flux Γ_i (#3, #17).

rent may appear at the first increase in time zone I. In this zone, $I_{N}{}^{+}$ and $I_{N2}{}^{+}$ increase as the current increases.

The first decrease in the ion collector current coincides with a decrease in the spectroscopic measurement of $I_{N}{}^{+}$ and $I_{N2}{}^{+}$. This can be explained as N^{+} and $N_2{}^{+}$ are consumed via reactions with the injected hydrogen neutrals, in accordance with [4];

$$N^{+} + H_2 \rightarrow NH^{+} + H, \quad (2)$$

$$N^{+} + H \rightarrow H^{+} + N, \quad (3)$$

$$N_2^{+} + H_2 \rightarrow N_2H^{+} + H. \quad (4)$$

The ions produced by these reactions are then consumed as follows:

$$N_2H^{+} + e^{-} \rightarrow N_2 + H, \quad (5)$$

$$N_2H^{+} + e^{-} \rightarrow NH + N, \quad (6)$$

$$NH_x^{+} + H_2 \rightarrow NH_{x+1}^{+} + H, \quad (7)$$

$$NH_x^{+} + e^{-} \rightarrow NH_{x-1} + H, \quad (8)$$

$$NH_{x-1} + e^{-} \rightarrow NH_{x-1}^{+} + 2e^{-}. \quad (9)$$

Through these reactions, some N^{+} and $N_2{}^{+}$ that may be produced in zone I become $NH_x{}^{+}$ and NH_x molecules. It is considered that the number of NH molecules would increase with the supply of hydrogen gas as I_{NH} is increased in zone II. NH_x molecules produced by these reactions become $NH_x{}^{+}$ through ionization and ion conversion. Therefore, the generation and disappearance balance of NH_x and $NH_x{}^{+}$, reactions (8) and (9), is important to explain the reaction process in zone II. It is difficult to quantitatively evaluate the impurity and hydrogen ion ratios from the ion collector current because of the complex situation where nitrogen and hydrogen gases are mixed. For a quantitative evaluation, the rate equations should be solved.

As depicted in zone III in Fig. 4 (c), the ion temperature does not change significantly. The increase in the ion current in time zone III can be attributed to the increased concentration of impurity ions. Note that the Larmor radius increases directly with the ion mass, as expressed in Eq. (1). The relative concentration of impurity ion species and their energy balance has to be addressed using dedicated numerical models, which will be discussed in the future.

Interestingly, the second increase in the ion collector current coincides with the maximum I_{NH}. The reaction process described above may increase NH. T_e during this time is ~10 eV (Fig. 4 (d) measured by #17), where the reaction coefficient for the ionization of NH_x is high (Fig. 5) and, thus, might explain the second bump in the ion collector to be due to an increase in $NH_x{}^{+}$. The ion flux rolls over (Fig. 4 (e)) when T_e at the same location drops below ~10 eV, i.e., at the beginning of zone III. Ion flux Γ_i follows the following relationship;

$$\Gamma_i \propto n_e \sqrt{\frac{k(\gamma T_{i\|} + T_e)}{m_i}}, \quad (10)$$

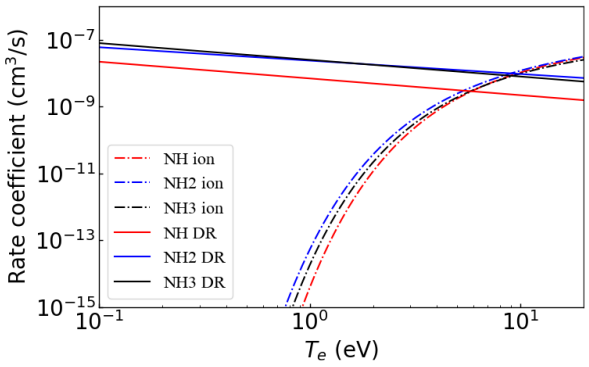

Fig. 5 Rate coefficients of the reactions of NH_x ionization and $NH_x{}^{+}$ Dissociative Recombination in Ref. [4].

where γ denotes the heat capacity ratio, $T_{i\|}$ denotes the ion temperature parallel to the magnetic field line, and m_i denotes the ion mass. $NH_x{}^{+}$ is heavy and may contribute to ion flux reduction. It is thought that impurity ions generated near the ISP flow into #3 at a slower velocity than the hydrogen ions, thereby affecting the ion flux of the probe in #3. As depicted in Fig. 4 (e), the decrease in n_e is smaller than that in Γ_i in zone III, which is in line with what has been observed in Ref. [8]. The reason for the difference in Γ_i reductions between the Langmuir probes #3 (Fig. 4 (e)) and #17 (Fig. 4 (f)) is related to the difference in T_e at the location of each probe (Fig. 4 (d)). The difference in T_e is thought to cause the difference in the #3 position, where recombination processes predominate from zone III, and the #17 position, where recombination processes predominate from zone IV.

The ion collector current decreases for the second time in zone IV, when T_e drops below ~8 eV. Below such a value, dissociative recombination becomes dominant over ionization, reducing the collected current. Furthermore, the seeding of H_2 and N_2 leads to a significant production of ammonia, NH_3, via plasma-wall reactions [17], which dissociate fast via electron impact to NHx in this electron temperature range. The time evolution of n_e in Fig. 4 (f) shows that n_e increases and then decreases within zone IV. This is in agreement with the change in the ionization/recombination balance discussed above.

4. Summary

This study investigates the effect of impurity ions on the ion current flowing into an ISP during the combined seeding of nitrogen and hydrogen gases in GAMMA 10/PDX. Different trends can be identified in the ion currents of Langmuir probes and the ISP installed in the D-module. Bumpy ion currents with two peaks are observed in the ion collector current of the ISP. The change in the current can be interpreted as depending on the type of ions reaching the electrode, because the ease of reaching the electrode varies depending on the difference in Larmor

radii due to the mass of the ion. By comparing this result with spectroscopic results, we attempt to estimate the impurity ion species. The increase in NH emissions coincides with the timing of the second bump, implying that the number of NH_x^+ produced by the N-MAR reaction process may be increased. The results of the time evolutions of the ion collector current of the ISP and spectral measurements obtained in this experiment can be explained as the interplay between ionization and recombination evolving in time according to plasma parameters at different spatial locations and impurity presence. These experimental results provide a further understanding of complex N-MAR processes in detached plasmas and may pose ISPs as an important diagnostic for future works in this reactor-relevant topic.

Acknowledgments

This work is partly supported by JSPS KAKENHI Grant Number 19K03790, 22H01198 and NIFS Collaboration Research program (NIFS19KUGM137, NIFS19KUGM146 and NIFS20KUGM148).

[1] A.W. Leonard, Plasma Phys. Control. Fusion **60**, 044001 (2018).
[2] N. Ohno, Plasma Phys. Control. Fusion **59**, 034007 (2017).
[3] A. Yu. Pigarov *et al*., Phys. Lett. A **222**, 251 (1996).
[4] R. Perillo *et al*., Plasma Phys. Control. Fusion **60**, 105004 (2018).
[5] R. Perillo *et al*., Nucl. Mater. Energy **19**, 87 (2019).
[6] R. Perillo *et al*., Phys. Plasmas **26**, 102502 (2019).
[7] N. Ezumi *et al*., Nucl. Fusion **59**, 066030 (2019).
[8] H. Gamo *et al*., Plasma Fusion Res. **16,** 2402041 (2021).
[9] A. Kallenbach *et al*., Plasma Phys. Control. Fusion **55,** 124041 (2013).
[10] N. Ezumi *et al*., AIP Conf. Proc. **1771**, 060002 (2016).
[11] Y. Nakashima *et al*., Nucl. Fusion **57**, 116033 (2017).
[12] M. Sakamoto *et al*., Nucl. Mater. Energy **12**, 1004 (2017).
[13] A. Terakado *et al*., Nucl. Mater. Energy **20**, 100679 (2019).
[14] K. Nojiri *et al*., Nucl. Mater. Energy **20**, 100691 (2019).
[15] I. Katsumata, Contrib. Plasma Phys. **36**, S 73 (1996).
[16] N. Ezumi, Contrib. Plasma Phys. **41**, 488 (2001).
[17] K. Sugiyama *et al*., Plasma Chem. Plama Process. **6**(2), 179 (1986).